Available online at www.sciencedirect.com
ScienceDirect
Journal of the European Ceramic Society 31 (2011) 999–1007
www.elsevier.com/locate/jeurceramsoc

Original Article

Effect of uniaxial load on the sintering behaviour of 45S5 Bioglass® powder compacts

Olivier Guillon [a,*], Shaoyong Cao [a], Jaemyung Chang [a], Lothar Wondraczek [b], Aldo R. Boccaccini [c]

[a] Ceramics Group, Materials Science, Technische Universität Darmstadt, Darmstadt, Germany
[b] Institute of Ceramics and Glasses, Department of Materials Science and Engineering, University of Erlangen-Nuremberg, Germany
[c] Institute of Biomaterials, Department of Materials Science and Engineering, University of Erlangen-Nuremberg, Germany

Received 8 October 2010; received in revised form 14 December 2010; accepted 21 December 2010
Available online 20 January 2011

Abstract

The effect of a uniaxial compressive load on the sintering behaviour of 45S5 Bioglass® powder compacts was investigated by means of sinter-forging. In comparison to free sintering, densification kinetics was enhanced and the degree of crystallization was reduced. Significantly lower sintering temperatures, i.e. 610 °C instead of 1050 °C, can be employed to obtain dense Bioglass® parts when sintering is performed under uniaxial load. The effect of mechanical loading on microstructure (pore density, shape and orientation) is discussed. The results of the investigation are relevant in connection with the development of sintered Bioglass® substrates for bone replacement devices, where both porosity and crystallinity of the part require careful control and low densification temperatures are sought.
© 2011 Elsevier Ltd. All rights reserved.

Keywords: Sintering; Glass; Crystallization; Microstructure-final; Biomedical applications

1. Introduction

In the family of biomaterials for orthopaedics and bone regeneration, bioactive glasses offer invaluable advantages over bioinert materials[1,2]: they promote bone regeneration by a number of chemical and biochemical reactions occurring at the interface between the implant and the human tissue. 45S5 Bioglass®, the oldest and most widely used material of the bioactive silicate glass family, of composition (wt.%) 45 SiO_2, 24.5 Na_2O, 24.5 CaO and 6 P_2O_5, was discovered by Hench in the late 60 s.[1] This material has found use and lately in the development of bone tissue engineering scaffolds.[3] The use of Bioglass® has been shown to activate the upregulation of genes in bone cells by controlled release of ionic products.[4] In the form of rigid implants for bone grafting or replacement, or scaffolds for tissue engineering, improved mechanical properties are required. This can be achieved by approaching theoretical density for the solid (struts in the case of scaffolds), reducing the defect size leading to fracture and eventually by controlling the crystallinity of Bioglass® derived glass-ceramics.[5] As shown by Clupper et al.[6] the hardness and fracture toughness of Bioglass® are indeed very moderate, typically 5 GPa and 1 MPa $m^{1/2}$, respectively, for a dense material. These properties are obviously reduced when the material is not fully dense.

A problem related to the sintering of 45S5 Bioglass® is that it tends to crystallize quickly above the glass transition temperature, impeding full densification by viscous flow. It was shown[7–10] that significant crystallization occurs already at ~580–650 °C, leading to an almost fully crystalline solid. Hence, much higher temperatures have to be applied to obtain sufficient further densification, typically above 1000 °C. Finally, at about 1200 °C the material melts. Sintering under mechanical load at low temperatures can help overcome this issue, by enhancing densification as well as by reducing the degree of crystallinity. According to Chevalier and Gremillard,[2] a lower degree of crystallinity may enhance glass bioactivity.

It is well known that a uniaxial or isostatic compressive stresses enhance the densification kinetics of materials sintering either by solid state sintering (diffusion processes), viscous flow or liquid phase sintering.[11–13] The additional pressure increases the vacancy gradients naturally occurring during free sintering by solid state sintering, leading to increased driving force for

* Corresponding author. Tel.: +49 (0) 6151 166396; fax: +49 (0) 6151 166314.
E-mail address: guillon@ceramics.tu-darmstadt.de (O. Guillon).

0955-2219/$ – see front matter © 2011 Elsevier Ltd. All rights reserved.
doi:10.1016/j.jeurceramsoc.2010.12.031

material transport along grain boundaries, help to redistribute matter by viscous flow from regions of high local pressure to regions of low pressure or to improve particle rearrangement when a liquid phase is present. Glass based materials are very sensitive to mechanical stresses applied during sintering, as evidenced by Ollagnier et al.[14] on Low Temperature Co-fired Ceramics and demonstrated in previous studies from dilatometric sintering data.[15] Stress induced anisotropy characterized by elongated pore shape and particular orientation could be observed in such materials. Furthermore, the use of mechanical loads may help to find a way to save energy in the process of sintering Bioglass®, by lowering drastically the temperature required for its densification by a few hundreds of degrees.

The aim of this paper is to characterize the effect of uniaxial loading on the macroscopic densification behaviour as well as microstructure evolution of Bioglass® powder compacts, when sintering by viscous flow and concurrent crystallization take place. To our knowledge, this has not been investigated yet for this class of materials in general (silicate systems prone to crystallization) nor for 45S5 Bioglass® in particular.

2. Experimental procedure

As a starting material, a glass of nominal composition (in wt.%) 24.5 Na_2O, 24.5 CaO, 6.0 P_2O_5 and 45.0 SiO_2 was prepared by conventional melting of a 1 kg batch of Na_2CO_3, $CaCO_3$, $Ca_3(PO_4)_2$ and SiO_2 (analytical grade) in a platinum crucible at 1500 °C for 1 h, using an electrical resistance furnace to avoid Pt dissolution in the glass melt. The composition of this glass equals that of Bioglass type 45S5. Glass frit was obtained by quenching the melt in water. The frit was subsequently crushed, ball-milled and finally ground in an attrition mill (EWTHV-0.5, Vollrath, Hürth, Germany) to obtain fine glass powder.

Powder density was measured by means of helium pycnometry (POROTEC GmbH), the particle size measured by high resolution SEM (XL30FEG, Philips). For that, 1 g of Bioglass® powder was dispersed in 5 ml ethanol under powerful ultrasonication (UP 200 s, Dr. Hielscher GmbH) for 1 min. The absence of crystallinity in the raw powder was checked by XRD (Bruker D8 Discovery) using Cu-K_α radiation, angular step $\Delta 2\theta = 0.02$ between 20 and 90° and a time per step of 4 s. Analysis of the XRD-diagram was carried out with X'Pert High Score software (Philips Analytical) using the PDF-Database-2004.

Cylindrical green bodies were obtained by dry pressing powder in two steps: first, a uniaxial pressure of 100 MPa was applied in a cylindrical matrix, followed by cold isostatic pressing under 250 MPa for 90 s. Two sizes of specimens were used: 10 mm diameter and height of 12 mm for high temperature dilatometric measurements at 1050 °C and 12 mm diameter and 14 mm height for the low temperature measurements at 610 °C. The green density was determined by the geometrical method.

The sintering experiments were carried out in a custom-made sinter-forging set-up, which has been described elsewhere.[16] A vertically split furnace mounted on a mechanical testing machine enabled to apply a well-controlled uniaxial load between 0 and 40 N via alumina pushrods. The load was kept constant during the whole thermal cycle from 400 °C and 590 °C, when the sintering temperature was 1050 °C and 610 °C, respectively. As densification does not start before 590 °C, this difference in the starting temperature does not induce any discrepancies in the results. Two laser scanners were used to measure in situ specimen height and diameter with a resolution better than 1 μm. From sample dimensions, strains were calculated and fitted with a polynomial function, which was derived to obtain strain rates as a function of density. A heating rate of 25 °C/min and dwell time of 120 min at the maximum temperature were chosen for all experiments. The contact surfaces between sample and alumina discs transferring the mechanical load were coated with a thin layer of boron nitride, to reduce friction during sinter-forging.

Sintered specimens were characterized as following: their density was measured by the Archimedes method, their crystallographic structure identified by means of the same XRD set-up described above (on the inner surface of cut specimens) and their microstructure examined by SEM on fracture surfaces and thoroughly polished sections (parallel to the loading direction, in the middle of specimens). To achieve better surface polishing, cut samples were embedded in an epoxy resin, which was thereafter thermally etched at 500 °C for 20 min. This allowed a better contrast between solid and pore phases under SEM. The image analysis was done using Image J software (NIH, USA). To prevent any bias from the binarization step, each pore was manually controlled before and after binarization. At least 350 pores (500 when pore orientation was characterized) were taken into account for each type of sample.

3. Results and discussion

The particles contained in the as-milled raw Bioglass® powder are angular due to the milling step and have a size between 0.5 and 10 μm, leading to an average particle size smaller than 5 μm. This is about the same size as for the powder used in previous studies.[7,9] Its density was determined as 2.85 g/cm^3 at 25 °C by helium pycnometry, and further taken as theoretical density under the assumption that no closed porosity was present in the measured particles. The same density was measured for the sintered crystallized sample at 1050 °C, indicating no significant effect of the crystallinity on the apparent density. This can be rationalized by the fact that the density of the principal crystal phase present in the heated samples ($CaNa_2Si_2O_6$) is 2.83 g/cm^3. No crystalline phase could be found from the XRD measurements, confirming the amorphous state of the raw powder.

3.1. Densification behaviour

The green samples had an average relative density of $\sim 70 \pm 1\%$, which is relatively high when using dry pressing as compaction method. Due to glass brittleness, the particle packing of the compact is likely to be enhanced by powder crushing, which may be a positive effect for the further sintering step. The axial and radial true strains measured during the high temperature cycle (up to 1050 °C) are plotted in Fig. 1. Curves for free sintering and sinter-forging under 1 and 5 N (corresponding to

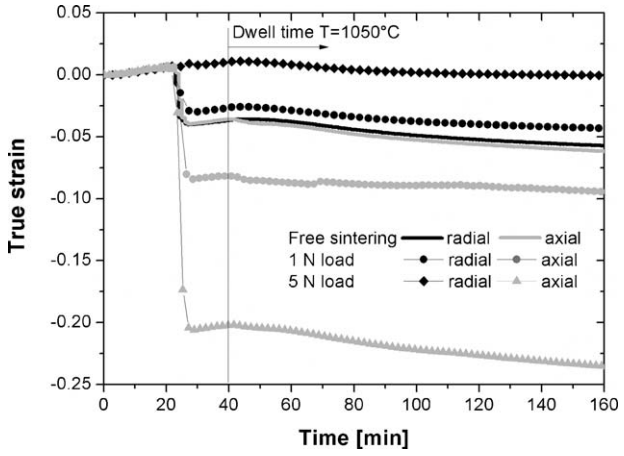

Fig. 1. Radial and axial strain curves measured by sinter-forging as function of the applied load (maximal temperature: 1050 °C).

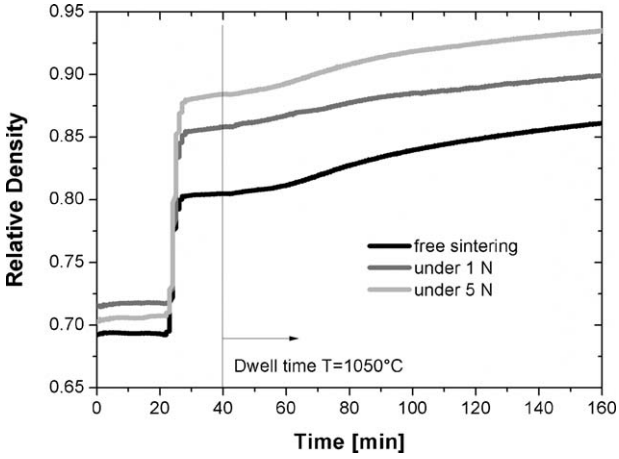

Fig. 2. Density curves as function of the applied load (maximal temperature: 1050 °C).

0.014 MPa and 0.073 MPa, respectively) are shown. For all data sets, after a linear thermal expansion step up to ~580 °C, the samples start to densify quickly up to about 700 °C and then show again linear thermal expansion behaviour without further densification. Only when reaching 1050 °C further shrinkage occurs with a reduced rate compared to the first stage. For free sintering, the first densification step is close to isotropic, with a linear shrinkage of ~4%. An additional 3% shrinkage can be gained after a dwell time of 2 h at 1050 °C. At the end of the process, noticeable shrinkage anisotropy can be measured, as $\varepsilon_r/\varepsilon_z = 0.93$, where ε_r is and ε_z are the radial and axial shrinkage strains, respectively. This anisotropic effect may be due to the initial particle orientation induced by uniaxial pressing, which nevertheless was not completely removed by the isostatic pressing step. The results for the free sintering experiments can be compared to data available in the literature on Bioglass® sintering. It appears that some similar characteristics can be observed, but also some discrepancies develop, especially at high temperatures. First, the temperature range and extent of the first densification step are in agreement with the work of Bretcanu et al.[9] and Lefebvre et al.[10] In the latter work, the extent of densification is larger, probably because of the smaller particle size used by Lefebvre et al.[10] (average particle size of 1.6 μm). With a heating rate of 20 °C/min, Bretcanu et al.[9] measured nevertheless further limited densification above 700 °C, which was not observed by Lefebvre et al.[10] nor in the present study. But the main difference between our work and the literature lies in the second densification step, which begins at about 850 °C for Lefebvre et al.[10] with a heating rate of 5 °C/min and at 950 °C for Bretcanu et al.[9] with a heating rate of 20 °C/min, which is much lower than for our experiments (start of second densification stage at 1050 °C with a heating rate of 25 °C/min). It seems that the higher the heating rate is, the higher the onset temperature for the second densification step is, as already observed up to 15 °C/min by Lefebvre et al.[10] This second densification step was attributed to a second glass transition of the remaining glass phase.[8] The corresponding glass transition temperature should however be constant and not change with the heating schedule. The reason for the observed discrepancies might be that the occurrence of viscous flow in the remaining glass phase is possibly hindered by the crystallites, whose amount and size depend on the heating schedule, initial particle size, and particle packing in the green compacts.

When applying a mechanical load, the degree of shrinkage anisotropy mentioned above was seen to increase, as expected from literature,[17] but the onset temperature for densification not. Even the smaller load of 1 N (~0.014 MPa) has a profound effect on the densification behaviour, promoting axial shrinkage while reducing radial shrinkage (final $\varepsilon_r/\varepsilon_z = 0.46$), as expected from literature results.[10–14] A load of 5 N (~0.073 MPa) is sufficient to inhibit radial shrinkage. Higher loads were found to lead to a barrelled specimen shape. Experiments carried out on a LTCC glass-ceramic material (SiO_2–Al_2O_3–CaO–B_2O_3 system) have shown a similar extreme sensitivity of densification to mechanical loading,[14] pressures of 0.02 MPa and 0.3–0.6 MPa being sufficient to induce shrinkage anisotropy and zero radial strain conditions, respectively. In earlier studies, the induction of shrinkage anisotropy in powder compacts sintered in dilatometers under low uniaxial loads has been also reported.[15] As a comparison, significantly higher stress levels are required to induce anisotropy in materials densifying by solid state sintering, like alumina.[18]

In order to compute relative density during the sintering cycle, the thermal expansion has to be removed from the total strain. It appears that the linear thermal expansion coefficient of Bioglass® is isotropic and it remains almost constant as determined from the densification-free segments (up to 550 °C, between 700 °C and 1000 °C and during cooling): $14.6 \times 10^{-6}\,K^{-1}$.

This value is in good agreement with the empirical prediction for a glass of equivalent composition using the SciGlass software package,[19] i.e. $15.1 \times 10^{-6}\,K^{-1}$.

Typical densification curves are shown in Fig. 2, for the same specimens as in Fig. 1. First, for free sintering, it appears that the first rapid densification step leads to a density of ~80%, whereas under load the achieved density is even higher, ~88%. The sudden stop in densification is attributed to the onset of crystallization of the Bioglass® particles, which has already been

reported in previous studies[8–10] and confirmed here by further XRD measurements. Under load very moderate increase in density can be observed between 700 °C and 1050 °C (up to 1% relative density). Interestingly, at 1050 °C, the further gain in density is more or less independent of the applied load. The crystallized material has a higher viscosity than the original glass composition (even at 1050 °C), hence the load has to be increased to observe any densification enhancement. The gain in final density measured for sinter-forged specimens comes almost totally from the first densification step, below 700 °C. To obtain fully dense specimens (instead of maximum 92% relative density under 5 N) a two step loading scheme could be conceived.

Scherer[11] developed a model for the densification of glass using a continuum mechanical description, according to the following equations:

$$\dot{\varepsilon}_r = \dot{\varepsilon}_{free} - \frac{\nu_p}{E_p}\sigma_z \quad (1)$$

$$\dot{\varepsilon}_z = \dot{\varepsilon}_{free} + \frac{1}{E_p}\sigma_z \quad (2)$$

where $\dot{\varepsilon}_{free}$ is the free strain rate, $E_p = 3\eta\rho[3\rho_{theo} - 2\rho]$ is the uniaxial viscosity and $\nu^p = (1/2)[\rho/(3\rho_{theo} - 2\rho)]^{1/2}$ the viscous Poisson's ratio. This framework, detailed and further developed by Olevsky,[20] enables to compute the compressive stress σ_z required to get zero radial shrinkage during sinter-forging:

$$\sigma_z = -\frac{\dot{\varepsilon}_{free} E_p}{\nu_p} \quad (3)$$

By combining Eqs. (1)–(3), the unknown scaling factor η can be calculated from the sinter-forging experiments by:

$$\eta = \frac{\sigma_z(1+\nu_p)}{12\nu_p^2(\dot{\varepsilon}_z - \dot{\varepsilon}_r)} \quad (4)$$

It can also be obtained from Eq. (3), if the stress required for zero radial shrinkage and free strain rate are known. Finally, for a density between 75% and 80%, the modelled stress lies between 0.07 and 0.08 MPa, which corresponds to the experiment with 5 N, suppressing any radial shrinkage. This confirms that the sintering behaviour of Bioglass® can be modelled by this continuum mechanical approach (at least for very low applied stresses). This was not the case for LTCC glass-ceramic compositions (e.g. see Ref. 14), for which large discrepancies between the isotropic model and experimental results were found, presumably due to development of large microstructural anisotropy.

According to these first results, a low temperature schedule was used, in order to focus on the first step of sintering and maximize it while reducing the degree of crystallization. Resulting strain curves are presented in Fig. 3. For free sintering, densification stops after ~10 min during the dwell time at 610 °C, probably due to the concurrent crystallization. A load of 10 N (~0.093 MPa) is sufficient to ensure zero radial shrinkage conditions, whereas a higher load of 40 N (~0.37 MPa) leads to expansion of the sample diameter during densification and axial strain of more than 40%. Nevertheless, even under load no further deformation is observed during the dwell time. As no data on isothermal sintering behaviour of Bioglass® powder has been

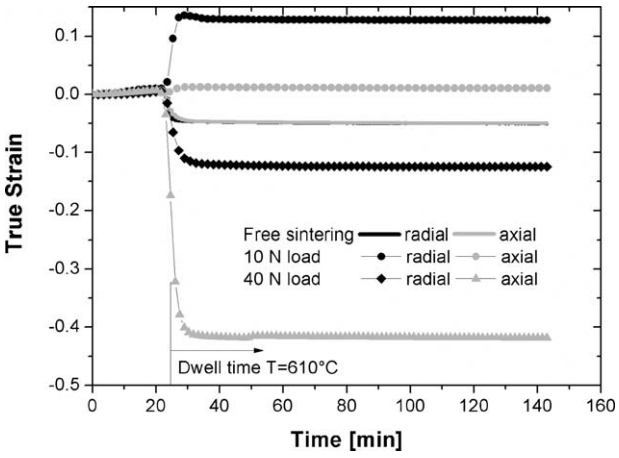

Fig. 3. Shrinkage curves as function of the applied load (maximal temperature: 610 °C).

reported in the literature, no comparison with previous experimental data can be made. It seems, however, that at 610 °C a degree of crystallinity preventing further densification even under 40 N may be quickly reached.

Resulting densification curves are plotted in Fig. 4. Under free sintering conditions the maximal density remained below 79% and at 1050 °C mechanical load increased densification. Under 40 N a maximal density of ~85% was reached, which is equal to the one obtained at 1050 °C under free sintering conditions.

3.2. Crystallization behaviour

Fig. 5 presents diffractograms obtained on different specimens. It confirmed the amorphous character of initial glass powder. Moreover it became apparent that the lubricant powder used (boron nitride) did not contaminate the samples during sintering, as shown by XRD analysis performed on bulk and at the contact surface with the pushrod.

The specimen sintered freely at 610 °C for 2 h show some rather weak and broad peaks related to the $CaNa_2O_6Si_2$ phase, which correlates well with previous results.[8,9,21] The amorphous

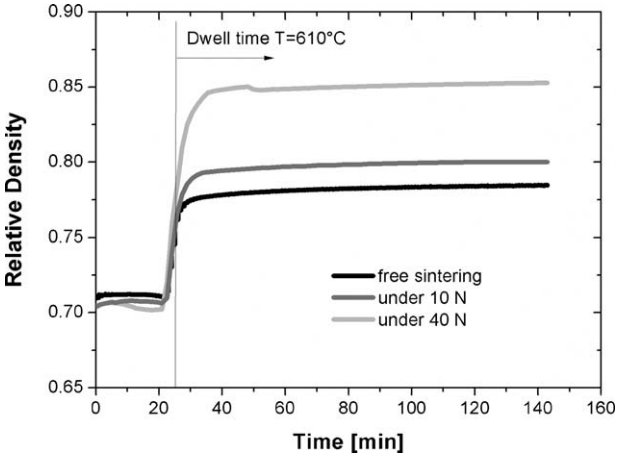

Fig. 4. Density curves as function of the applied load (maximal temperature: 610 °C).

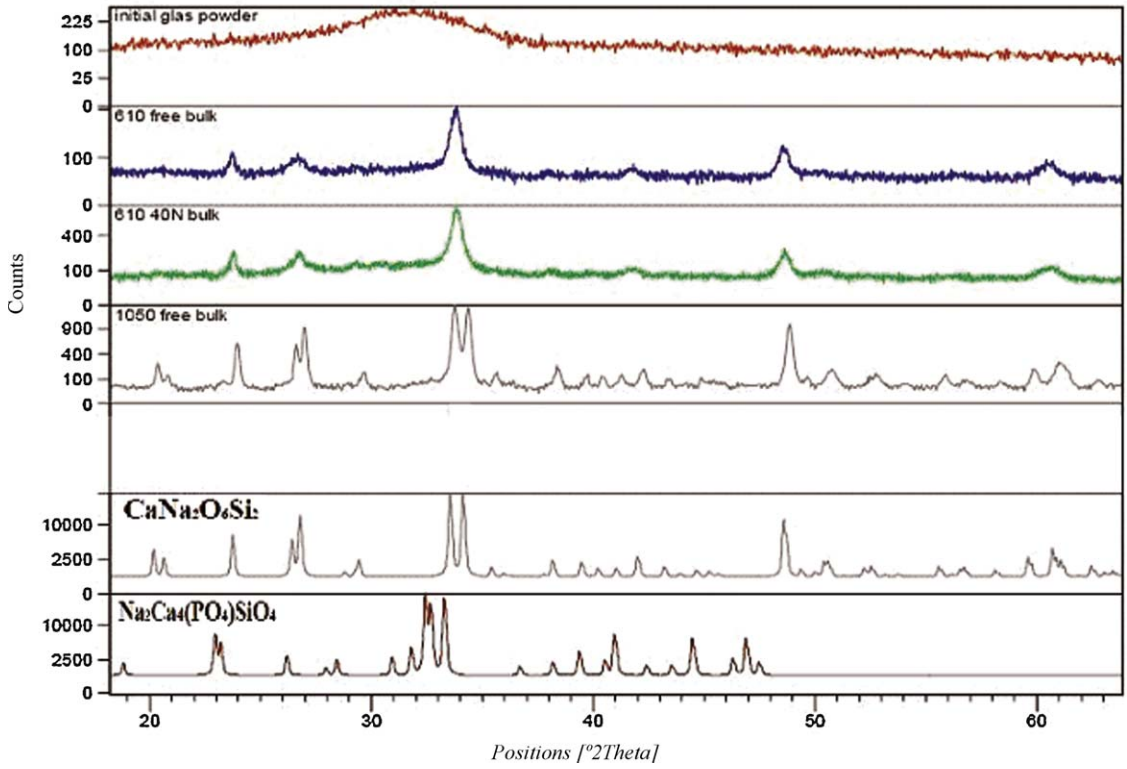

Fig. 5. XRD measurements for different specimens.

hump in the 2θ range $25^\circ < 2\theta < 40^\circ$ is still noticeable. As a comparison, the XRD spectrum of a sinter-forged specimen sintered under 40 N is displayed: peak position and amplitude are similar, which means that this level of applied stress primarily affects densification kinetics. The crystallization process as such and, hence, the type of precipitated crystal species, on the other hand, are assumed to remain unaffected by pressure within the considered pressure regime. Typically, significantly higher stress levels would be required to affect phase stability in glass.[22–24]

Double peaks present at $2\theta \sim 34^\circ$ and 26° in the standard diagram merged into one single peak in the investigated specimens. This may be related either to the small size of the crystallites leading to a broadening of diffraction peaks or to the distortion of the lattice cell. Similar behaviour was observed by Boccacini et al.[21] as function of temperature. Above 800 °C double peaks were observed and additional characterization with better resolution techniques would be required to highlight the progressive variation of the lattice parameters. Nevertheless, the Scherrer's formula can be used to estimate the $CaNa_2Si_2O_6$ rhombohedral crystallite size x from high intensity single peaks (for example at $2\theta \approx 48.9^\circ$):

$$x = \frac{k\lambda}{\beta \cos\theta} \quad (5)$$

where k is the Scherer's constant for spherical crystallites ($k = 0.9$), λ the wavelength of the Cu-K_α radiation (1.5406×10^{-10} m), and β is the full width at half maximum of the considered peak. This gives an average size $x = 16$ nm. As a comparison, Lefebvre et al.[8] using the same equation evaluated the $Na_2CaSi_2O_6$ crystal size to be 18 nm after heating at 650 °C, and 35 nm at 850 °C. Fracture surfaces under SEM such as the one shown in Fig. 6a indicate that fine crystals develop on the surface of glass particles, as proposed by Clupper and Hench.[7] They found for a similar initial particle size an Avrami exponent of 1 which means that a surface crystallization mechanism is dominant for Bioglass®. More recently, Bretcanu et al.[9] also confirmed this result.

At 1050 °C, the main crystalline phase is still $CaNa_2Si_2O_6$ but a very weak signal originating from the phosphorus rich phase $Na_2Ca_4(PO_4)_2SiO_4$ can be seen in the XRD pattern. This analysis is confirmed by the fracture surface in Fig. 6b, for which a few of these elongated orthorhombic crystals can be observed. The fracture mode is no longer conchoidal, which conveys the idea that the body is crystallized to a large extent, as evidenced by the strong and clear XRD reflection peaks. Similarly to the finding on samples sintered at 610 °C, no differences are observed in the diffractograms between sinter-forged and freely sintered specimens are found.

3.3. Microstructure characterization

Typical microstructures of sintered specimens are shown in Fig. 7. After binarization with Image J software, the pore distribution was analyzed, as shown in Table 1. The global porosity content correlated well (within 1%) with density values measured by the Archimedes method, confirming the suitability of the evaluated snapshots as well as the reliability of the image analysis method used.

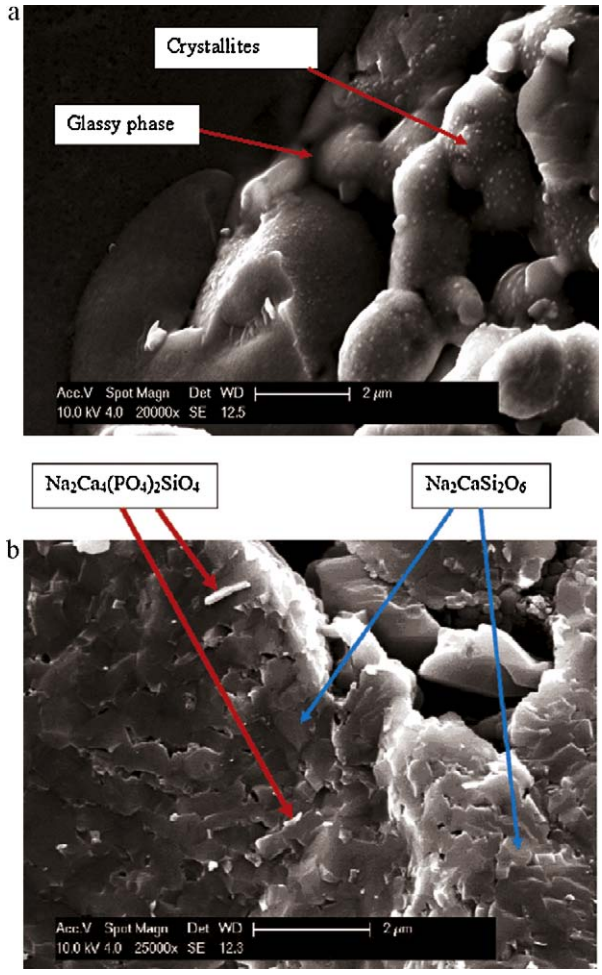

Fig. 6. SEM of fractured surfaces (a) free sintering at 610 °C and (b) free sintering at 1050 °C.

It was found that the number of pores per unit area increases with relative density, either achieved by higher sintering temperatures or applied loads. It is usually expected from simplified micromechanical sintering models that the number of pores remains constant for a unit cell throughout the sintering process.[25] For real and more heterogeneous materials, this may not be the case. It was for example observed on alumina layers that the number of pores per area decreases for densities above 90%,[26] meaning that smaller pores disappear. Here, on the opposite, the number of pores per unit area increases significantly especially for the specimens sinter-forged at 1050 °C. Nevertheless, this result has to be correlated with the typical pore size, characterized by the average area of the pore sections. It appears that pore size is also largely affected by temperature as well as applied load. On one hand, samples sintered at 610 °C have large pores (cross sectional area of around 30 μm^2) when sintered freely but by applying a compressive load of 40 N, the pore area decreases down to less than 5 μm^2. As at the same time relative density and number of pores per unit area increases, this means that uniaxial loading leads to the closing of large and complex shaped pores and their division into smaller ones. The same trend is also seen at 1050 °C, whereas the initial mean pore area for free sintered samples is already smaller than that measured at 610 °C. High temperature sintering and mechanical loading lead both to refinement and homogenization of the microstructure and enhanced densification. Nevertheless, mechanical pressure seems to be more efficient in reducing pore size than sintering temperature, as for the same density, specimens sintered at 610 °C under 40 N have a mean pore area about half of the one measured for samples freely sintered at 1050 °C.

The crystallization occurring at the surface of particles at 610 °C seems to be highly detrimental to pore closure, as the viscous flow may be hindered by deposits of crystals on the glass particle free surfaces. Opposite to glass-ceramic composites, for which rigid inclusions are mixed in the glassy matrix in the bulk, the hindrance of viscous flow here leads to a heterogeneous microstructure composed of large voids covered by crystalline phase and homogeneous dense regions which had properly densified. As shown in Fig. 7, these solid regions are up to 50 μm long, which means that they are more than 10 times the initial particle size. The uniaxial mechanical load contributes to the reduction of the largest pores, as the specimen sintered under 40 N at 610 °C has a maximal pore cross sectional area of 110 μm^2 and the specimen sintered freely at 1050 °C with the same final density is characterized by pores of 303 μm^2 in cross sectional area. Besides that, pore circularity (being equal to 1 for a perfect circle) increases with density achieved by sinter-forging. Again, this is simply explained by the fact that pores in less densified specimens have a complex shape. The positive effect of sinter-forging on the reduction of flaw size and number was already reported by Boutz et al. on tetragonal zirconia.[27]

For densities at least equal to 85%, pore sections were assimilated to ellipses, whose aspect ratio and orientation could be quantified. Only pores with an aspect ratio (major axis divided

Table 1
Characteristics of pore distributions (dwell time 2 h).

Sintering temperature [°C]	1050			610		
Load [N] (stress [MPa])	0 (0)	1 (0.014)	5 (0.073)	0 (0)	10 (0.093)	40 (0.37)
Pores per unit area [pore/μm^2]	0.020	0.047	0.043	0.008	0.010	0.014
Average pore area [μm^2]	8.09	3.04	2.24	28.27	12.87	4.62
Average pore circularity	0.61	0.87	0.88	0.53	0.56	0.63
Proportion of elongated pores	0.97	0.48	0.55	–	–	0.99
Average pore aspect ratio	2.61	1.55	1.56	–	–	2.63
Pore orientation factor *k*	0.40	0.43	0.39	–	–	0.53
Relative density	0.85	0.89	0.93	0.78	0.81	0.85

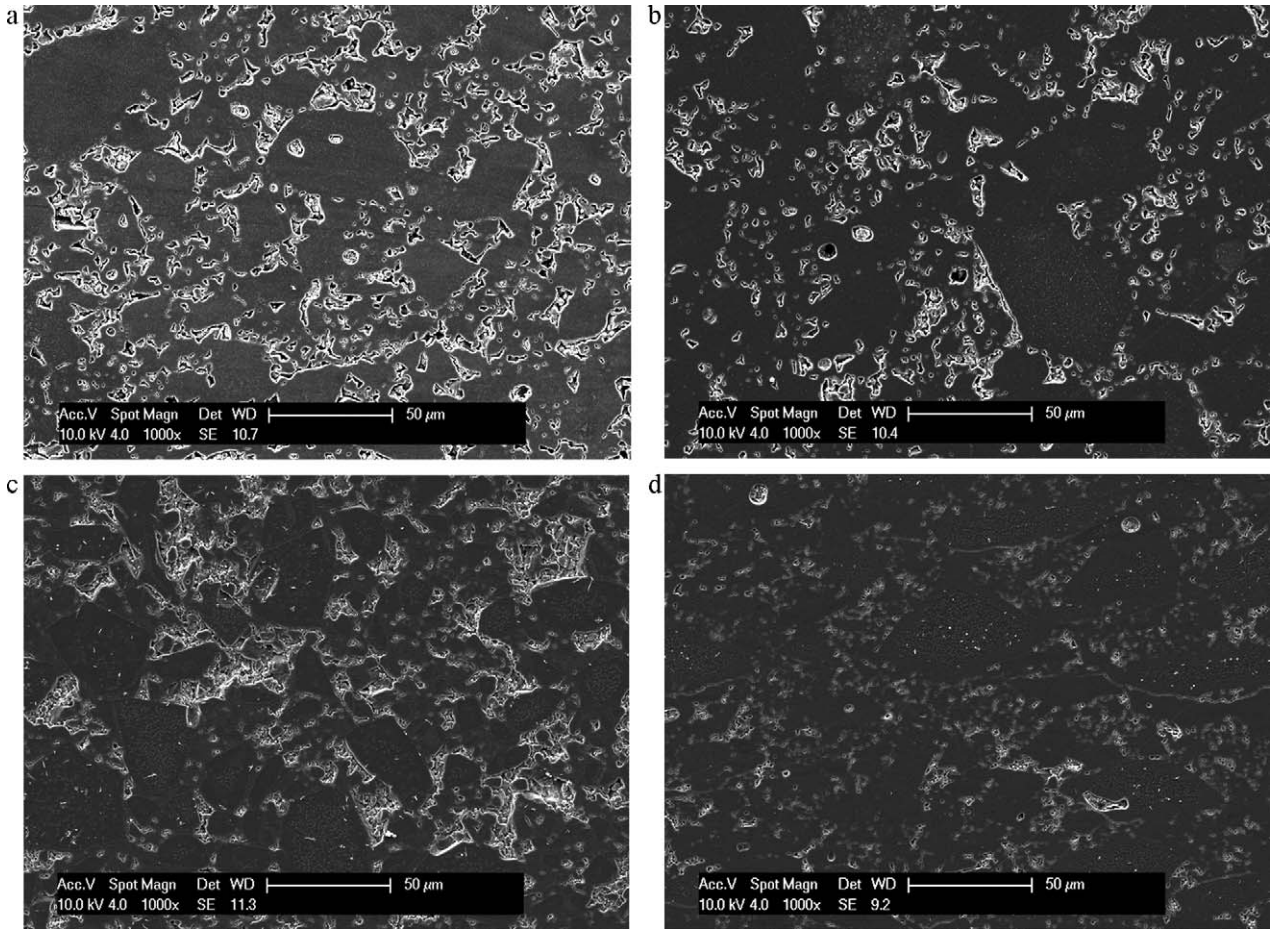

Fig. 7. Polished and thermally etched cross sections (vertical axis is the loading direction, dwell time 2 h): (a) freely sintered at 1050 °C, (b) under 5 N at 1050 °C, (c) freely sintered at 610 °C and (d) under 40 N at 610 °C.

by minor axis) larger than 1.05 were considered for this further evaluation. It appears that for 85% of density, independently of the way this density was reached, almost all pores are highly anisometric, as shown in Table 1. Similar aspect ratio values were found for the specimen sintered freely at 1050 °C and the one sinter-forged at 610 °C. Pore orientation may however by affected by the uniaxial pressure, as discussed below. On the other hand, for higher densities obtained under compressive loading at 1050 °C, only about half of the pores exhibit measurable anisotropy; therefore the average is smaller (aspect ratio ~1.5).

The pore orientation distribution was calculated adding the pore maximal Feret's diameter multiplied by its aspect ratio along different angle ranges.[28] First, all anisometric pores were taken into account, without consideration of their size, as shown in Fig. 8. Qualitatively, pores are less oriented along the loading direction than normal to it, especially for the specimen sintered under 40 N at 610 °C. Here a clear pore orientation can be defined, apparently larger than for specimens sintered at 1050 °C. In order to quantify pore orientation, the pore orientation factor k was defined as the cumulated pore length lying perpendicularly to the applied load (angle segments 0–30° and 150–180° divided by the total pore length between 0 and 180°). In a randomly oriented isotropic material, a value of 0.3 would be expected. The higher values presented in Table 1 found for all specimens mean that there is a preferred pore orientation normal to the loading direction. As expected, the largest value is found for the specimen sintered under the largest load (40 N) at 610 °C. The other specimens sintered at 1050 °C have a similar pore orientation ($k \sim 0.4$), indicating that the applied load of 5 N does not have a significant effect on pore orientation.

It was experimentally observed that for zirconia (8YSZ) densifying by solid state sintering, there is a critical pore size above which pores deform according to the macroscopic strain state by creep.[29] Below this critical size, small pores were found to align consistently along the loading direction, as necks under compression grow faster. This asymmetrical neck growth rate leads indirectly to an oriented anisometric porosity in sinter-forging oxides.[30] This critical size was about 2 times the particle size in the case of 8YSZ, under an applied load of 1 MPa. In the case of glass, such a critical pore size may be questionable. Even if no well defined pore geometry was artificially introduced in the present specimens, the pore orientation distribution was also calculated for pores larger than the 80% fractile of the pore section distribution p80 (i.e. the 20% largest pores). No clear trend can be derived from these new distributions, except that large pores are more likely to be aligned horizontally during free sintering at 1050 °C. Additional characterization

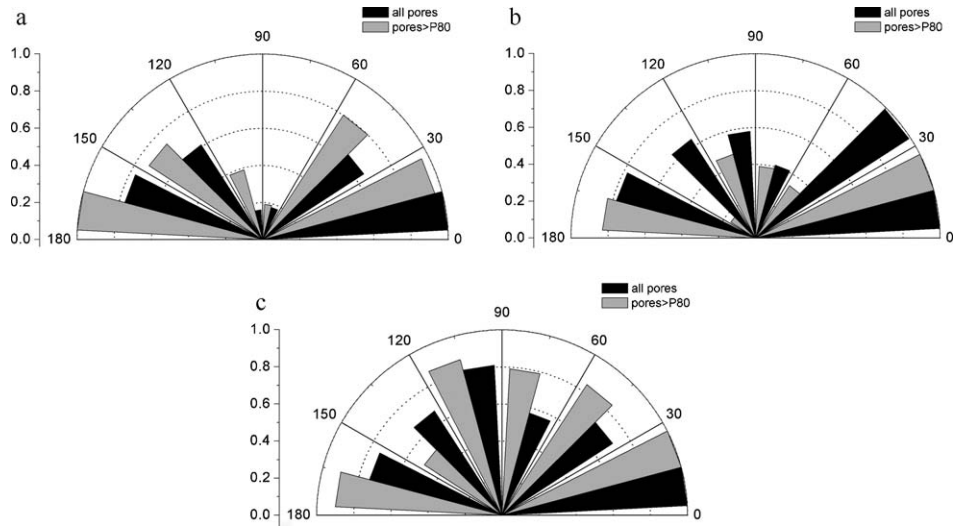

Fig. 8. Pore orientation distribution (90° is the loading direction, dwell time 2 h): (a) under 40 N at 610 °C, (b) freely sintered at 1050 °C and (c) under 5 N at 1050 °C.

with artificial spherical defects may be of interest to tackle this question.

4. Conclusions

The effect of uniaxial loads on the sintering of 45S5 Bioglass® powder compacts was investigated by means of sinter-forging experiments. During free sintering at low temperature (610 °C), densification stops quickly due to surface crystallization which hinders viscous flow of the glass. A second densification step takes place only by further heating up to 1050 °C. However, application of a very moderate compressive load enables to densify Bioglass® powder compacts possibly preventing radial shrinkage at 610 °C. By assisting densification, the uniaxial load homogenises the microstructure, reducing the mean pore size and at the same time increasing the pore number by division. In addition, pores tend to flatten perpendicularly to the load direction under stress. To reach final densities larger than 90%, a temperature of 1050 °C is not required (as is the case for free sintering samples). The maximum of anisotropy is met at a relative density of 85%. Anisotropic microstructure seems to develop during the first low temperature densification step and disappears with further densification, even under load, at 1050 °C.

References

1. Hench LL. Bioceramics – from concept to clinic. *J Am Ceram Soc* 1991;**74**(7):1487–510.
2. Chevalier J, Gremillard L. Ceramics for medical applications: a picture for the next 20 years. *J Eur Ceram Soc* 2009;**29**(7):1245–55.
3. Chen QZ, Thompson AID, Boccaccini AR. 45S5 Bioglass®-derived glass-ceramic scaffolds for bone tissue engineering. *Biomaterials* 2006;**27**:2414–25.
4. Hench LL, Day DE, Höland W, Rheinberger VM. Glass and medicine. *Int J Appl Glass Sci* 2010;**1**(1):104–17.
5. Peitl O, Oréfice RL, Hench LL, Brennan AB. Effect of the crystallization of bioactive glass reinforcing agents on the mechanical properties of polymer composites. *Mater Sci Eng A* 2004;**372**:245–51.
6. Clupper DC, Hench LL, Mecholsky JJ. Strength and toughness of tape cast bioactive glass 45S5 following heat treatment. *J Eur Ceram Soc* 2004;**24**(10–11):2929–34.
7. Clupper DC, Hench LL. Crystallization kinetics of tape cast bioactive glass 45S5. *J Non-Cryst Solids* 2003;**318**:43–8.
8. Lefebvre L, Chevalier J, Gremillard L, Zenati R, Thollet G, Bernache-Assolant D, Govin A. Structural transformations of bioactive glass 45S5 with thermal treatments. *Acta Mater* 2007;**55**(10):3305–13.
9. Bretcanu O, Chatzistavrou X, Paraskevopoulos K, Conradt R, Thompson I, Boccaccini AR. Sintering and crystallisation of 45S5 Bioglass® powder. *J Eur Ceram Soc* 2009;**29**(16):3299–306.
10. Lefebvre L, Gremillard L, Chevalier J, Zenati R, Bernache-Assolant D. Sintering behaviour of 45S5 bioactive glass. *Acta Biomater* 2008;**4**:1894–903.
11. Scherer GW. Viscous sintering under a uniaxial load. *J Am Ceram Soc* 1986;**69**(9):C206–7.
12. Rahaman MN, Dejonghe LC, Scherer GW, Brook RJ. Creep and densification during sintering of glass powder compacts. *J Am Ceram Soc* 1987;**70**(10):766–74.
13. Zuo R, Aulbach E, Rödel J. Experimental determination of sintering stresses and sintering viscosities. *Acta Mater* 2003;**51**(15):4563–74.
14. Ollagnier J-B, Guillon O, Rödel J. Effect of anisotropic microstructure on the viscous properties of a LTCC material. *J Am Ceram Soc* 2007;**90**(12):3846–51.
15. Boccaccini AR. Shrinkage anisotropy of glass powder compacts sintered in dilatometers. *J Mater Res* 1998;**13**(6):1693–7.
16. Aulbach E, Zuo R, Rödel J. Laser-assisted high-resolution loading dilatometer and applications. *Exp Mech* 2004;**44**(1):71–5.
17. Boccaccini AR, Olevsky EA. Anisotropic shrinkage during sintering of glass-powder compacts under uniaxial stresses: qualitative assessment of experimental evidence. *Met Mater Trans A* 1997;**28A**:2397–404.
18. Wonisch A, Guillon O, Kraft T, Moseler M, Riedel H, Rödel J. Stress-induced anisotropic behaviour of sintering alumina: discrete element modelling and experiments. *Acta Mater* 2007;**55**(15):5187–99.
19. *SciGlass Glass Property Information System, SciGlass 7.4*; 2010. http://www.sciglass.info/.
20. Olevsky EA. Theory of sintering: from discrete to continuum. *Mater Sci Eng R* 1998;**23**:41–100.
21. Boccaccini AR, Chen Q, Lefebvre L, Gremillard L, Chevalier J. Sintering, crystallization and biodegradation behaviour of Bioglass®-derived glass-ceramics. *Faraday Discuss* 2001;**136**:27–44.
22. Gutzow I, Durschang B, Rüssel C. Influence of pressure and shear flow on the crystallization behaviour of a glass melt based on the $Li_2Si_2O_5$-composition. *J Mater Sci* 1997;**32**:5405.

23. Wondraczek L, Sen S, Behrens H, Youngman RE. Structure-energy map of alkali borosilicate glasses: effects of pressure and temperature. *Phys Rev B* 2007;**76**:1–8, 014202.
24. Wondraczek L, Mauro JC. Advancing glasses through fundamental research. *J Eur Ceram Soc* 2009;**29**:1227–34.
25. Rahaman MN. *Ceramic processing and sintering*. Marcel Dekker AG; 2003.
26. Guillon O, Nettleship I. Microstructural characterization of alumina films during constrained sintering. *J Am Ceram Soc* 2010;**93**(3): 627–9.
27. Boutz M, Winnubst L, Burggraaf A, Nauer M, Carry C. Low temperature sinter-forging of nanostructured Y-ZTP and YCe-TZP. *J Am Ceram Soc* 1995;**78**(1):121–8.
28. Guillon O, Weiler L, Rödel J. Anisotropic microstructural development during the constrained sintering of dip-coated alumina thin films. *J Am Ceram Soc* 2007;**90**(5):1394–400.
29. Frame, D. PhD thesis, University of Washington; 2006.
30. Zuo R, Aulbach E, Bordia RK, Rödel J. Critical evaluation of hot forging experiments: case study of alumina. *J Am Ceram Soc* 2003;**86**(7):1099–105.